CAV2001:sessionA4.001

Evaluation of Cavitation Erosion based on Erosion Particles

S.Hattori and E.Nakao,

Department of Mechanical Engineering, Faculty of Engineering, Fukui University 9-1 Bunkyo 3-Chome, Fukui 910-8507, Japan

Pacific Special Alloy Coatings Co., Ltd ., Naoetsu Works, 2-25-1 Minato-cho, Joetsu-shi, Niigata 942-0011, Japan

Abstract

Cavitation erosion mechanisms were studied through the observation of removed particles for annealed S15C (equivalent to AISI 1015) steel and heat-treated S55C (AISI 1055) steels. In the initial and the incubation stages, single impact loads removed many small sharply-edged particles. During the acceleration and the maximum rate stages, large striated particles were observed due to cyclic loads. The volume fraction of particles exhibiting fatigue fracture in these stages amounts to 70 or 80% irrespective of the material including pure copper and pure aluminum. The exponent of the crack growth rate determined from the fracture is almost the same as that obtained from a regular fatigue test. The fatigue crack growth rate for many metals is inversely proportional to the square of Young's modulus, E^{-2}. The particles fall off from the protrusive surface and their sizes depend on the unevenness in relation to the hardness of the material. The average diameter of erosion particles decreases inversely with the square root of Vickers hardness, $HV^{-1/2}$. Therefore, the volume is proportional to $HV^{-3/2}$. Thus, the dependence of the volume loss rate in the maximum rate stage is well described by $HV^{-3/2}\cdot E^{-2}$. The conclusion is that cavitation erosion can be evaluated in terms of the hardness of the material and the fatigue crack growth rate.

1. Introduction

Cavitation erosion has been evaluated quantitatively based on parameters such as cumulative mass loss, cumulative volume loss and cumulative mean depth of penetration (Hattori et al., 1985), yet these parameters are insufficient to fully describe the mechanisms of cavitation erosion. Microscopical studies (Wade et al., 1978) have been carried out by scanning electron microscopy to identify the dominating factors of cavitation erosion, but only qualitative discussions were possible. Therefore, other methods of observation should be employed in order to estimate cavitation erosion mechanisms and to evaluate the cavitation damage quantitatively. One method is to observe erosion particles, because those give evidence of the fracture characteristics and the quantitative amount of damage.

Endo et. al (Endo et al., 1969) carried out cavitation erosion tests and found that the diameter of many large erosion particles is in the range of less than 10μm in the initial and more than 30μm in the maximum erosion rate stage. The former stage erosion is due to impact fracture and the latter stage due to fatigue fracture. Okada et. al (Okada et al., 1977) found that in the initial stage angular erosion particles are removed due to impact fracture. The authors believe that it is just important not to determine the dominating factor, but to consider the simultaneous occurrence of both types of fracture. That is, cavitation erosion should be evaluated by taking into account the ratio of impact and

fatigue fracture.

On the other hand, many researchers have tried to correlate the cavitation erosion with properties of the material. For example, Hobbs(Hobbs, 1967)and Heymann (Heymann, 1970) attempted to correlate the erosion resistance with various forms of strain energy derived from tension tests on the same materials. The best correlation was obtained with the "ultimate resilience" (that is the limiting strain energy beyond the elastic limit) expressed as (1/2)(tensile strength)^2/elastic modulus. However, this parameter of the material was found not to be universal, i.e. it did not fit the erosion resistance of all materials. This is because the parameters were derived from static tension tests, while cavitation erosion occurs through dynamic fracture modes. Therefore, the erosion should be evaluated in terms of parameters including the kind of fracture mechanism.

In the present study, the size distribution of erosion particles moving into the test solution during cavitation erosion tests were analyzed. The fracture mechanisms were clarified quantitatively based on particle analyses. Moreover, the crack growth forming an erosion particle was measured, and the erosion rate was evaluated, considering the formation of erosion particles.

2. Test Specimen and Test Procedures

The test materials were the carbon steels 0.15%C (equivalent to AISI 1015), 0.55%C (AISI 1055), pure aluminum and pure copper. The chemical compositions, heat treatment and mechanical properties are listed in Tables 1 and 2. The test surface of each specimen was polished with an emery paper and then was buff-finished.

The test apparatus was a magnetostrictive vibratory device. The test specimen was screwed to the free end of an amplifying magnetostrictive vibrating horn (open beaker method ASTM G32). The diameter of the test specimen and the horn frequency were 16mm and 19.5kHz, respectively. The double amplitude (peak to peak) was 50μm. The test liquid was ion-exchanged water kept at 25±1°C.

After exposure to cavitation, the test specimen was removed from the vibrating horn, and weighed by a precision balance with a sensitivity of 0.01mg. The amount of cavitation erosion was obtained as volume loss rate, which is mass loss divided by the density of the specimen's material and by the test duration. The eroded surface was observed by scanning electron microscopy.

Table 1 Chemical compositions of the test materials [wt.%]

	C	Si	Mn	P	S	Cu	Ni	Cr
S15C	0.15	0.25	0.47	0.015	0.013	0.14	0.04	0.18
S55C	0.55	0.27	0.82	0.016	0.017	0.02	0.02	0.09

	Si	Fe	Cu	Mn	Mg	Cr	Zn	Ti	Al
Al	0.09	0.14	0.01	0.01	0.01	0	0.01	0.01	Bal.
Cu			99.96						

Erosion particles were collected on a plastic filter through which the test solution passed

Table 2 Heat treatment and mechanical properties of the materials

Material	Heat treatment	Density [kg/m^3]	Young's modulus [GPa]	Vickers hardness [HV]
S15C	600℃, 30 min vacuum annealed	7.87×10^3	206	130
S55C	600℃, 30 min vacuum annealed	7.87×10^3	206	220
	850℃, 30 min oil quenched + 550℃, 60 min tempered			310
	850℃, 30 min oil quenched + 400℃, 60 min tempered			410
Al	As received	2.71×10^3	71	33
Cu	As received	8.96×10^3	129	90

under low downstream pressure. The vacuum pressure was 33.3kPa. The filter paper was a porous polycarbonate membrane, which was the same as Ahamed et.al used (Ahmed et al., 1991). Erosion particles on the filter were coated with vapored gold, and then observed by scanning electron microscopy. For the element analyses of the erosion particles, an X-ray microanalyzer (Horiba LTD, EMAX-1770) was used. After taking photographs of erosion particles, the particles were traced by hand on a paper in order to increase the black and white contrast and finally measured, using an image analyzer (Nippon Avionics Co., LTD, TVIP2000).

3. Experimental Results and Discussion

3.1. Time Dependence of Cavitation Damage

Figure 1 shows the volume loss rate curve of S15C steel over time. The process can be divided into four subsequent stages (Hattori et al., 1985). There is an initial stage (b) characterized by high volume loss rate at the beginning of the test, an incubation stage (c) with low volume loss rate, an acceleration stage (d) and a maximum rate stage (e). The eroded surface of each stage is shown in Fig.2. The specimen surface was etched in a 3% HNO_3 alcohol solution before conducting the erosion test. The photos were all taken at the same location. No significant change is observed between Figs.2(a) and (b). Only an angular pit with a size of 3μm is formed by cleavage fracture due to the single impact load as shown in the magnification of Fig.2(b'). In the incubation stage of Fig.2(c), many slip bands were observed on ferrite grains, and some cracks indicated by the arrow A originate along the slip bands as a result of the accumulating plastic deformation. No notable deformation occurs in pearlite, and some steps are formed with ferrite. In the acceleration stage of Fig.2(d), plastic deformation accumulates and removal of material is observed in many locations. Some areas still preserve their original surface in this stage. In the maximum rate stage of Fig.2(e), the original surface is completely removed. The highly deformed surface layer appears to be broken into small pieces, which drop one after another into the test solution. This explains the constant volume rate in this stage. Thus, the eroded surface suggests that cavitation erosion can be produced by fatigue fracture. That is, the erosion proceeds in a sequence of steps such as slip band

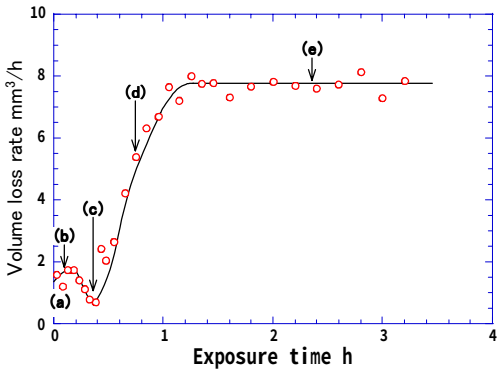

Fig. 1 Volume loss rate curve of S15C

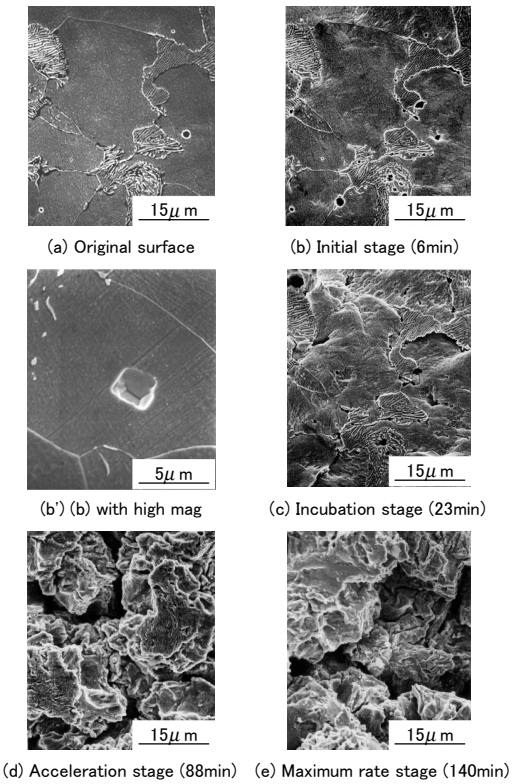

Fig. 2 Eroded surfaces of S15C

initiation, accumulation of plastic deformation, crack initiation, growth and particle removal.

The shape and size of erosion particles were examined in order to discuss the cavitation erosion mechanisms. Figure 3 shows typical particles observed in the initial stage and the maximum rate stage. In the initial stage, particles are characterized by a flat surface and sharp edges of about 3μm in size. The particles have almost the same size and shape as those of the pits observed on the eroded surface and shown in Fig.2(b'). Besides many small particles, one observes in the maximum rate stage large particles with fatigue striation.

Table 3 shows the distribution of the particle sizes. The sizes were measured on five SEM photographs with a magnificatio n of 1,000 and 4,000, respectively. The photos were taken at random locations on the filter. The measuring area was $6.0\times10^4\mu m^2$, equivalent to the sum of five sheets of photos at a magnification of 1,000. The particles were elliptic, and the diameter was defined as the average of the major and minor axes. It has been reported (Okada et al., 1977) that the diameter of the most frequently removed particles becomes large in the maximum rate stage, compared with in the incubation stage. In this study, however, the diameter of the most frequently removed is in the range from 0.3 to 1μm in every stage and the numbers decrease exponentially with the diameter. This is because the size of about 400 particles collected through centrifugation (starting with the largest ones and omitting smaller particles beyond the counting limit of 400) were measured in the previous report al (Okada et al., 1977). In this study, many particles including small ones could be collected on the porous plastic filter. It can be seen from Table 3 that the maximum diameter is between 8 or 9μm in the initial and the incubation stages, and about 15μm in the acceleration and maximum rate stages. The number of particles less than 4μm in diameter decreases in the incubation stage and the following stages. The Vickers microhardness on the surface was measured, as shown in Fig.4. The hardness increases with exposure time up to 15 minutes, and then reaches a constant value. The increase is due to the work hardening the surface layer, which is consistent with the decreased number of small particles in Table 3.

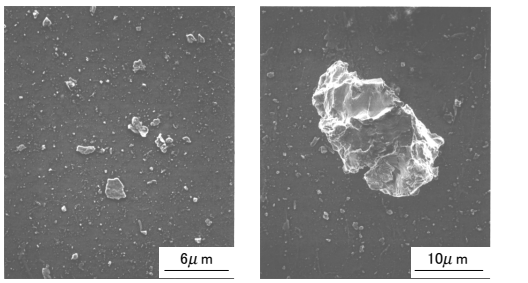

(a) Initial stage (5min) (b) Maximum rate stage (140min)

Fig. 3 SEM microphotographs of erosion particles

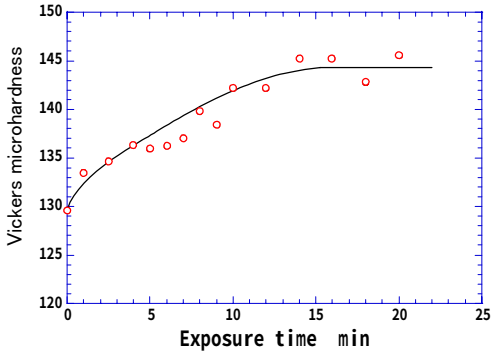

Fig. 4 Variation hardness of S15C

Table 3 The number of erosion particles, Measuring area : 6.0×10^4 mm^2

Particle diameter[μm]	0.3–1	1–2	2–3	3–4	4–5	5–6	6–7	7–8	8–9	9–10	10–11	11–12	12–13	13–14	14–15	15–16	16–17	Total number
Initial	4066	287	160	60	27	11	4	3										4618
Incubation	3096	187	63	21	0	9	5	0	1									3382
Acceleration	3335	272	78	13	8	7	5	5	0	2	0	1	1					3727
Maximum rate	2671	289	49	10	6	4	3	2	2	1	3	0	2	0	1	0	1	3044

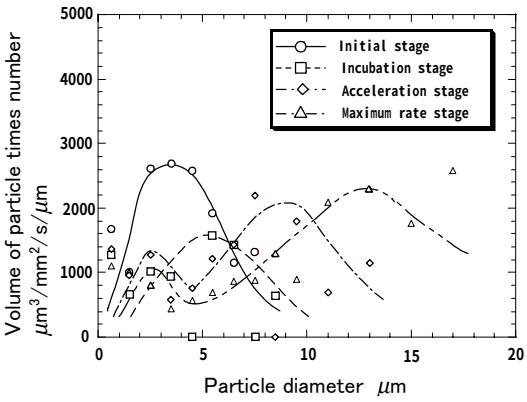

Fig. 5 Relation between particle diameter and erosion volume of S15C

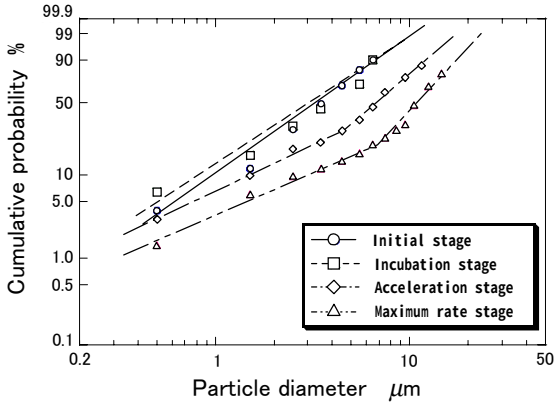

Fig. 6 Weibull distribution of erosion volumes as function of particle diameter (S15C)

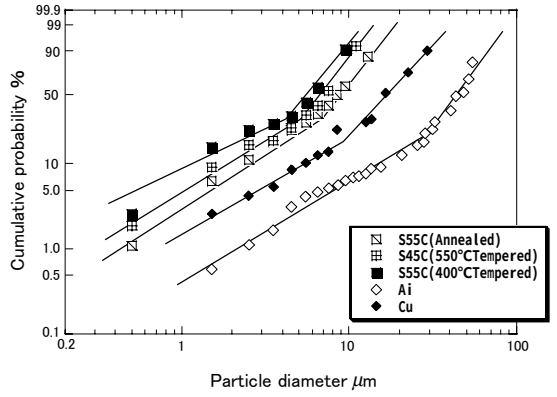

Fig. 7 Weibull distribution of erosion volumes as function of particle diameter

The erosion particles were correlated with the volume loss. Figure 5 shows the relation between particle diameter and erosion volume. The erosion volume was defined as the volume of particles multiplied by the number, which was calculated from Table 3. The erosion particles were assumed to be spherical in shape and the volume was deduced from the particle diameter. In the initial stage, the erosion volume curve has a single peak. Many angular particles with a diameter of 3 to 5μm were observed. Therefore, in this stage, erosion is stirred by impact fracture. In the incubation stage, the curve has a single low-value peak to be explained by the work hardening the surface layer. In the acceleration stage, two peaks appear and the second peak is due to the removal of large particles produced by slow crack growth in the highly deformed surface layer. The large particles have surfaces with a fatigue striation and now, the controlling factor is fatigue fracture. In the maximum rate stage, the particle diameter at the second peak is observed to be about 14μm. The increase in diameter indicates the dominance of fatigue fracture at this stage. Still, many particles with a diameter of less than 5μm are removed in the acceleration and the maximum rate stages, which means that in every stage impact fracture occurs continuously.

Figure 6 shows the Weibull distribution of the erosion volumes as function of the particle diameter. A straight line can be drawn through datapoints in the initial or the incubation stage. Bent lines (duplex type Weibull distributions) can be drawn both in the acceleration and the maximum rate stage. The duplex type Weibull distribution shows that two separate fracture mechanisms exist and the transition occurs at the cuspidal point. This means that material removal occurs simultaneously through impact and fatigue fracture. The percentage of fatigue fracture of the entire erosion is 75% in the acceleration stage and is 80% in the maximum rate stage.

In order to examine the material dependence on the percentage of fatigue fracture, similar measurements were performed for heat-treated S55C steel (equivalent to AISI 1055 steel), pure aluminum and pure copper. Figure 7

shows the Weibull distribution of erosion volumes obtained in the maximum rate stage. All metals have duplex type Weibull distributions and the ratio of fatigue fracture is 70% to 80% independent of the kind of material.

3.2. Evaluation of Volume Loss in Terms of Erosion Particles

Since the volume loss rate in the maximum rate stage is more than 6 times higher than that in the initial or the incubation stage, the volume loss in the maximum rate stage was discussed here in terms of erosion particles.

The volume loss should be evaluated by taking into account the fracture mechanisms. Figure 8 shows the material removal from the protrusive surface in the maximum rate stage. The experiments were carried out using the two-half test specimen method (Okada et al., 1994). That is, the specimen, which had been cut into two pieces, was clamped together and exposed to vibrating cavitation (stationary specimen method). The exposed specimen was again released into two pieces and the cross section of the pieces was observed by scanning electron microscopy. This procedure was repeated. Fig.8(a) shows the cross section of the specimen exposed for 2 hours in order to reach the maximum rate stage. Two cracks begin to appear at the bottom of the groove; the downward one is about 6μm long and the right downward inclined one is about 0.5μm. After 3 min., the downward crack did not grow, but the inclined crack propagated up to 2μm and it elongated up to 4μm, exposed for 3 more min. Finally, material removal occurred after another 3 min.

Figure 9 shows the variation in crack length. The crack growth rate is low when the crack is small, and increases with the crack length. The relation between crack length a and crack growth rate da/dt is shown in Fig.10. The relation is very similar to the ΔK-(da/dN) relation obtained from a regular fatigue test (Paris et al., 1963). The crack growth rate da/dN from the fatigue test can be expressed as

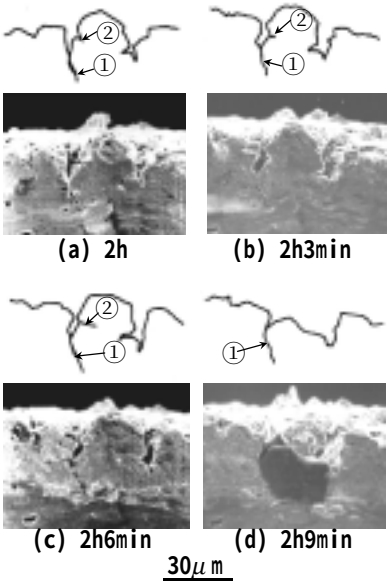

Fig. 8 Crack observed on cross-section of eroded surface

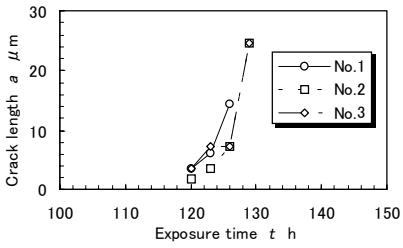

Fig. 9 Variation in erosion crack length

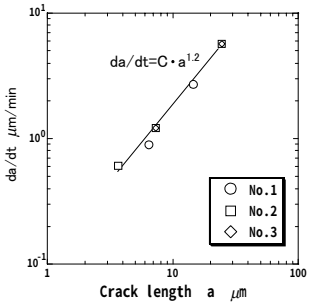

Fig. 10 Relation between crack length and crack growth rate

$$da/dN=C\cdot(\Delta K)^m \quad (C\text{: constant}), \tag{1}$$

where the stress intensity range ΔK is given by

$$\Delta K=\Delta\sigma\sqrt{\pi a}\ . \tag{2}$$

Unfortunately, the stress intensity range ΔK at the tip of cracks on eroded surfaces exposed to cavitation is not known. If the stress amplitude $\Delta\sigma$ could be assumed to be constant a nd the number of cycles to be proportional to the exposure time, then da/dt could be defined as

$$da/dt=C\cdot a^{0.5m}. \tag{3}$$

The exponent of the above equation, $0.5m$, is found to be 1.2 as seen in Fig.10. Therefore, the value of m reduces to 2 .4. The value is reasonable, because an exponent m of 2 to 4 has been obtained for carbon steels from fatigue tests (Paris et al., 1963). This means that the material removal in cavitation erosion tests occurs by way of fatigue. This finding can be applied to the open beaker method as described in the previous section 3.1.

The volume loss rate can be expressed as a function of particle size and removal rate. Since the removal rate depends on the crack growth rate, the removal rate of various metals was discussed here including pure copper and pure aluminum. Speidel (Speidel, 1973) reported the relation between fatigue crack growth rate da/dN and $\Delta K/E$ (E:Young's modulus) to be independent of the kind of material and expressed it as

$$da/dN=C'\cdot(\Delta K/E)^2 \quad (C'\text{: constant}). \tag{4}$$

Therefore, if ΔK is constant, da/dN will be proportional to the reciprocal of E^2.

On the other hand, the average particle diameter corresponds to the depth of the eroded uneven surface, which depends on the hardness of the material. Figure 11 shows the relation between Vickers hardness and the mean diameter of erosion particles, which was calculated by using the weight law (Franc et al., 1997), i.e.

$$D_w=\Sigma D_iV_i/\Sigma V_i, \tag{5}$$

where D_i is the diameter of a particle and V_i is the volume of a particle. This figure shows that the mean diameter is proportional to $HV^{1/2}$.

Since the volume of a particle becomes proportional to $HV^{3/2}$ and the removal rate is proportional to E^{-2}, the volume loss rate by fatigue fracture V_{fa} can be given by

$$V_{fa}\propto HV^{3/2}\cdot E^{-2}, \tag{6}$$

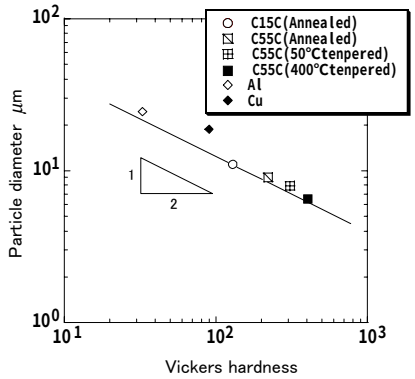

Fig. 11 Relation between Vickers hardness and erosion particle diameter

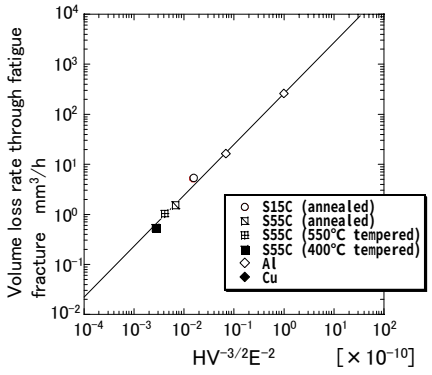

Fig. 12 Relation between $HV^{-3/2}$ E^{-2} and volume loss rate

expressing V_{fa} as product of maximum volume loss rate and ratio of fatigue fracture. Figure 12 shows the relation between $HV^{-3/2}\cdot E^{-2}$ and the volume loss rate in a double logarithmic plot. A straight line with a gradient of one is obtained. The correlation factor is 0.99. Consequently, the cavitation erosion in the maximum rate stage can be evaluated in terms of the material hardness and the fatigue crack growth rate.

4. Conclusions

The following conclusions can be drawn.

(1) Impact fracture is the dominating factor for the erosion in the initial and incubation stages. In the acceleration and the maximum rate stages, fatigue fracture occurs in addition to impact fracture. In the maximum rate stage, the percentage of fatigue fracture is 70% to 80% independent of the kind of material.

(2) The crack growth rate of the eroding surface in the maximum rate stage can be expressed as

$da/dt=C\cdot a^{1.2}$,

t: exposure time, C: constant, a: crack length.

The value of the exponent, 1.2 is very similar to that obtained from regular fatigue tests.

(3) The volume loss rate in the maximum rate stage has a good correlation with $HV^{-3/2}\cdot E^{-2}$. That is, the volume loss rate can be evaluated in terms of the material hardness and the fatigue crack growth rate.

References

Ahmed, S. M., Hokkirigawa, K., Kikuchi, K., Higuchi, J., and Oba, R., 1991, "SEM Studies of Particles Produced by Cavitation Erosion," *Transactions of the Japan Society of Mechanical Engineers*, (in Japanese), Vol.57, No.1237, pp. 2873.

Endo, K., Okada, T., and Baba, Y., 1969, "Fundamental Studies on Cavitation Erosion," *Bulletin of JSME*, Vol.12, No.52, pp. 729

Franc, J. P., and Michel, J. M., 1997, "Cavitation Erosion Research in France : the State of the Art," *Journal of Marine Science and Technology*, pp.233.

Hattori, S., Sun, B. H., Hammitt, F. G., and Okada, T., 1985, "An Application of Bubble Collapse Pulse Height Spectra to Venturi Cavitation Erosion of 1100-O Aluminum," *Wear*, Vol.103, pp.119-131.

Heymann, F. J., 1970, "Toward Quantitative Prediction of Liquid Impact Erosion," *ASTM STP*, Vol.474, pp.212.

Hobbs, J. M., 1967, "Experience with a 20-kc Cavitation Erosion Test," *ASTM STP*, Vol. 408, pp.159

Okada, T., Iwamoto, J., and Sano, K., 1977, "Fundamental studies on Cavitation Erosion (Observation of the Eroded Surface by Scanning Electron Microscope)," *Bulletin of JSME*, Vol.20, No.147, pp.1067.

Okada, T., Iwai, Y., and Fukuda, Y., 1994, "Formation and Progression of Cavitation-Erosion Surface," *Transactions of the Japan Society of Mechanical engineers*, (in Japanese), Vol.60, No.570, pp. 563.

Paris, P. C., and Erdogan, F., 1963, *Trans. ASME*, Vol.85, pp.528.

Speidel, M. O., 1973, *Intern. Conf. SCC and HE of Metallic Materials.*

Wade, E. H. R., and Preece, C. M., 1978, *Metallurgical Transaction A*, Vol.9A, pp.1299.